Study on the Dynamic Aerodynamic Performance of Airfoil with Direct Force Measurement

Yuqin Jiao, Chunsheng Xiao, and Dengke Wu

Abstract An in-depth study on the dynamic aerodynamic performance of the pitching oscillating airfoil is carried out in the two-dimensional test section of the NF-3 low-speed wind tunnel of Northwestern Polytechnical University. The experimental model is a span-wise three-section force measuring model, and the force measure is only performed in the middle section of the model to reduce the influence of the sidewall interference of the wind tunnel. In the experiment, the transient angle of attack of the model is collected, the inertial force and pitching moment on the middle section of the model are calculated, and the data collected from the balance is subtracted to correct the influence of the model's inertia on the results. The results show that the angle of attack exceeding the positive or negative static stall angles of attack is a necessary condition for the lift and pitch moment coefficients to produce a large hysteresis loops. As the oscillation reduced frequency increases, the dynamic stall is delayed, the lift coefficient hysteresis loop increase, the drag coefficient increase, and the pitch moment coefficient near the maximum angle of attack decrease. When the angle of attack is less than the static angle of attack of stall or exceeds a small range, with the increase of the reduced frequency of the airfoil oscillation, the pitch moment coefficient of the airfoil decreases when it goes up and increases when it goes down. With the increase of the oscillation amplitude, the hysteresis loops of both dynamic lift coefficient and pitching moment coefficient of the oscillating airfoil increase. As the average angle of attack increases, the angle of attack of airfoil enters the positive stall zone more, the lift coefficient hysteresis loop increases, and the minimum pitch moment coefficient decreases. The Reynolds number has no obvious effect on the hysteresis loop of lift, drag and pitch moment coefficients; however, in the downward process, as the Reynolds number increases, the lift recovery advances, and the hysteresis loop decreases.

Keywords Airfoil · Wind tunnel test · Dynamic aerodynamic performance · Direct force measurement · Inertia correction

Y. Jiao (✉) · C. Xiao · D. Wu
National Key Laboratory of Science and Technology on Aerodynamic Design and Research, Northwestern Polytechnical University, No.127 Youyixi Road, Beilin, Xi'an, Shaanxi, China
e-mail: jiaoyuqin@nwpu.edu.cn

1   Introduction

The maneuverability requirements of fighter jets, the study of the dynamic characteristics of helicopter rotors and wind turbines in the field of wind energy all require more in-depth research on the dynamic aerodynamic performance and dynamic stall characteristics of the airfoil [1–3]. In the 1940s, Himmelskamp first discovered the existence of dynamic stalls in experiments, but it was not until the study of helicopter rotor experiments in the 1960s that the study of dynamic stalls received attention [4–9]. A variety of test methods have been applied to dynamic stall research to measure lift, drag, pitching moment and related flow parameters and flow characteristics during the stall. The commonly used measuring methods for dynamic stall research include: (1) using dynamic pressure sensors to measure airfoil surface pressure [6, 7, 9–11], (2) using Hot-Wire probes [6, 7, 12] or Particle Image Velocimetry (PIV) measure the velocity field around the airfoil [13–15], and (3) using the direct force measurement to study the influence of various airfoil motion parameters on its dynamic aerodynamic performance [12, 16–19]. The surface pressure measurement can only obtain the differential pressure drag, and the results of lift and pitch moment also have larger errors. Although the direct force measurement cannot obtain the detailed information of the flow field, it can better obtain the dynamic aerodynamic performance data of the airfoil.

The measurement results of the aerodynamic balance in the dynamic force measuring test include a certain amount of inertial force and pitching moment. In order to eliminate this error, in the above-mentioned direct force measuring study, a test with the pitching oscillation of airfoil is usually carried out without running of the wind tunnel (i.e., wind-off) before the formal test, and then the test with the same pitching oscillation of airfoil is performed under the required test wind speed in the wind tunnel (i.e., wind-on). And then, the wind-on data subtract the wind-off data, which is considered to eliminate the influence of the inertial force and pitching moment under the required test wind speed. Since the airfoil model is still subjected to aerodynamic forces even though the wind tunnel is not being driven, this method of eliminating the influence of inertia has errors. The National Key Laboratory of Science and Technology on Aerodynamic Design and Research of Northwestern Polytechnical University has carried out research on this issue. By accurately measuring the transient angle of attack of the model movement during the wind tunnel test, calculating the inertial force and pitching moment and correcting the test data, it has been verified that the inertial influence has been successfully corrected. In this paper, the direct force measurement is used to study the dynamic aerodynamic performance of a wind turbine airfoil with a relative thickness of 18% with both Reynolds number of millions and sinusoidal pitch oscillation.

2   Descriptions of Experiments

2.1   Experimental Equipment and Instruments

The experiment was carried out in the two-dimensional test section of the NF-3 low-speed wind tunnel of the National Key Laboratory of Science and Technology on Aerodynamic Design and Research of Northwestern Polytechnical University. This wind tunnel is low-speed open circuit wind tunnel of the all-steel structure and of length of 80 m, which power is 1120 kw. The two-dimensional test section has a rectangular cross-section of 8 m long, 3 m wide and 1.6 m high. The maximum wind speed is 130 m/s, the minimum steady wind speed is 10 m/s for the empty wind tunnel, the axial static pressure gradient is $dCp/dx = 0.0011(1/m)$ and airflow turbulence is $\varepsilon = 0.045\%$.

The model oscillating motion driving mechanism is composed of a DC motor, a large flywheel, a reducer, a "-|"-shaped rod, an adjustable connecting rod and a swing lever. The DC motor with tachometer drives the "-|"-shaped rod, adjustable connecting rod and swing lever through a large flywheel and reducer to make the model to reciprocate in the sinusoidal law in the air flow of the test section. The motor is the Z4-132–3 type DC speed-adjusting motor with a rated power of 18.5 kW, a rated rotation speed of 1540 rpm, and a maximum rotation speed of 3000 rpm. The cylindrical worm reducer model is WHC18, which reduction ratio is 8, and the oscillation frequency range of airfoil model is 0–5 Hz. It is shown through theoretical analysis and experimental verification that the maximum deviation between the mechanism and the theoretical sinusoidal pitching oscillation motion angles is less than 0.146% (Fig. 1).
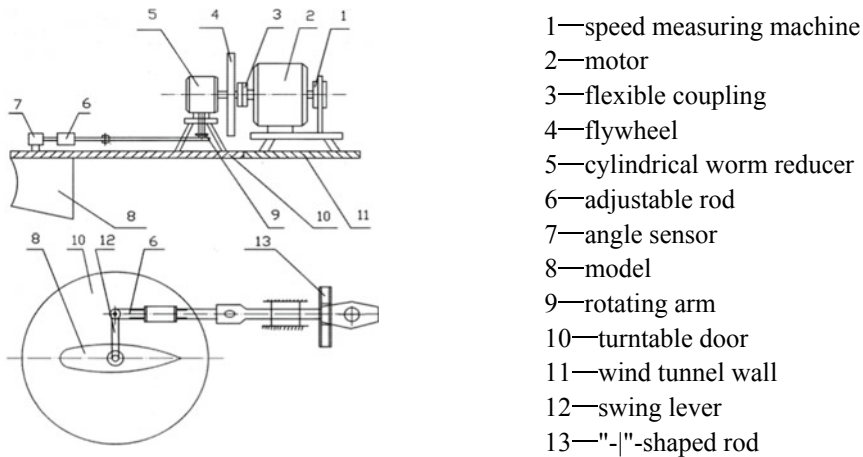

1—speed measuring machine
2—motor
3—flexible coupling
4—flywheel
5—cylindrical worm reducer
6—adjustable rod
7—angle sensor
8—model
9—rotating arm
10—turntable door
11—wind tunnel wall
12—swing lever
13—"-|"-shaped rod

Fig. 1   Schematic diagram of model oscillating motion driving mechanism

Table 1 Load capacity and static calibration performance index of balance

Item	Y	X	Z	M_z
Design load (N, N·m)	2200	600	500	200
Calibration load (N, N·m)	2000	500	500	200
Absolute error (N, N·m)	8	1.2	1	0. 7
Static calibration (%)	0.3	0.2	0.2	0.35
Limit error (%)	0.9	0.6	0.6	1.05
Comprehensive accuracy (%)	0.1	0.06	0.04	0.1

The aerodynamic force measurement uses a four-component box-type airfoil aerodynamic balance, which laboratory number is YXTP-4. The measuring components are lift Y, drag X, lateral force Z, and pitching moment Mz. The overall dimensions of the balance are 150 mm in length, 65 mm in width and 77 mm in height. The design center of the balance is 36.5 mm from the bottom. The balance material is high-strength aging steel 00Ni18Co8Mo5TiAl (Table 1).

An angle sensor is installed on the model shaft rotation. In the experiment, the signal of angle sensor and the four-component signals vi the balance are collected by the dynamic measurement module of the Agilent VXI E8401A data acquisition system. The dynamic measuring performance index are that there are 32 measurement channels, each channel can be independently sampled in parallel, the range can be set independently, the acquisition speed of each channel is 100 kHz, there is a 16-bit independent A/D converter and the input signal voltage range is ±12.5 mV ~ ±10.0 V. The dynamic measuring accuracy of the system is better than 0.1% FS.

2.2 Experimental Model

The experimental model uses a 18% thick wind turbine airfoil with a span of 1.6 m and a chord length of 0.6 m. The overall frame span-wise three-section structure is used, and the upper and lower sections of the airfoil model are directly processed on the overall frame [20]. The upper and lower sections of the model adopt the structure with the support plates and outer skin, the interior is hollow, the outer skin is made of glass fiber reinforced plastic, the thickness is 5 mm, and the support plates are wing-shaped metal or fiberboard (Fig. 2). The middle section of the model is made up of upper and lower parts, which are made of high-strength, low-density 7075 aluminum alloy, and suspended on the overall frame of the model through the balance (Fig. 3). This not only ensures the overall strength and stiffness of the model, but also minimizes the mass and moment of inertia of the model in order to increases the oscillation frequency and reduced frequency during the test. The weight of the middle section of the processed model is 13.5 kg, the position of the center of gravity of the middle section of the airfoil model is $x_G = 216.41$ mm, $y_G = 13.71$ mm, and $z_G = -9.74$ mm.
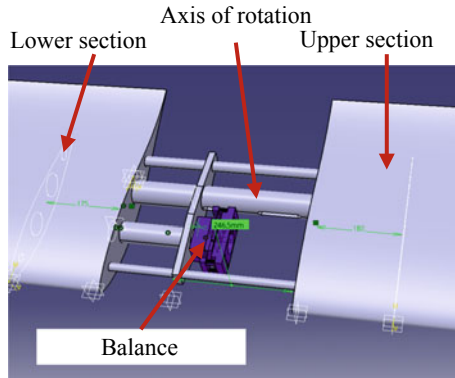
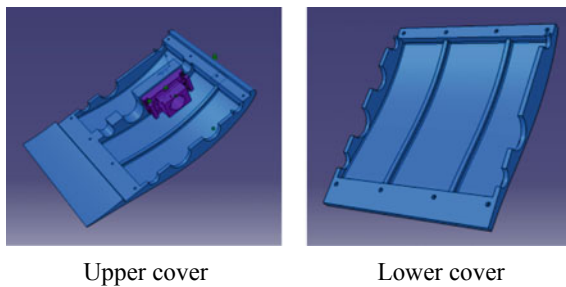**Fig. 2** Structure diagram of the airfoil dynamic force measuring model

Fig. 3 The upper and lower cover of the middle section of the airfoil model

The experimental model is vertically suspended between the upper and lower turntables of the two dimensional test section of the wind tunnel. The upper and lower rotation shafts of the model are supported in the center holes of the turntables with bearings and can rotate flexibly. The upper rotation shaft reaches out through the center hole of the upper turntable and connects with the model pitching oscillating motion driving mechanism.

3 Elimination Method of Inertial Force and Pitching Moment

In the airfoil dynamic force measuring experiment, the airfoil model performs sinusoidal pitch oscillation driven by the driving mechanism, and the middle section of the model is driven direct by the aerodynamic balance. The force and pitching moment measured by the balance include both the aerodynamic force and pitching moment on the middle section of the model by the flow field and the inertial force

and pitching moment of the middle section of the model. It is necessary to evaluate the inertial force and pitching moment of the middle section of the airfoil model and correct the direct force measuring results.

3.1 Elimination of Inertial Pitching Moment

When the center of gravity of the middle section of the airfoil model is on the model's axis of rotation, as shown in Fig. 4, because the middle section of the model only produces a inertial pitching moment on the balance while model move as pitching oscillation about the model's axis of rotation, and no inertial forces are generated in the x-axis direction and the y-axis direction. Of course, the moment reference center of the aerodynamic balance often does not coincide with the axis of rotation of the model and when the inertial force and pitching moment is deducted, the measured value is first converted to the coordinate system with origin at the axis of rotation of the model. For the force balance installed in the middle of the model in this article, the moments measured and transmitted by the balance are similarly

$$M_{z,b} = M_{z,d} = M_z + I_z \ddot{\alpha} \tag{1}$$

where $M_{z,d}$ and $M_{z,b}$ are the driving pitching moment and the pitching moment measured by the balance, which have been translated to a coordinate system centered on the axis of rotation according to the principle of coordinate system translation, α is the pitching oscillation transient angle of attack, t is the time, and $\ddot{\alpha}$ is the second derivative of the transient angle of attack α with respect to time t, and I_z is the moment of inertia of the middle section of the model around the axis of rotation parallel to the z-axis. Therefore, the aerodynamic pitching moment acting on the model is
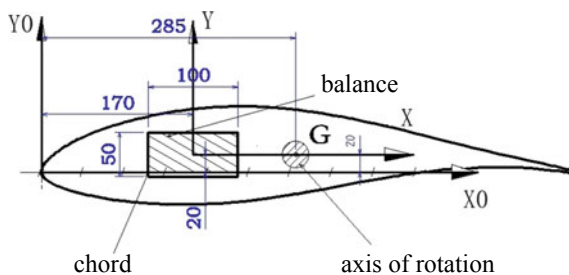
$$M_z = M_{z,b} - I_z \ddot{\alpha} \tag{2}$$

Fig. 4 Sectional diagram of the middle section of the model (the center of gravity G of the model on the axis of rotation of model)

The moment of inertia I_z is obtained by the Compound Pendulum Method and $Iz \approx 0.3505$ kg·m^2.

3.2 Elimination of Inertial Force

As shown in Fig. 5, when the center of gravity of the middle section of the model G is not on the central axis of rotation and the model rotates around the axis of rotation, it is subjected to centrifugal force. This centrifugal force is included in the measuring values of the built-in aerodynamic balance in this article. Of course, as above-mentioned in Sect. 3.1, the measured value is first converted to the axis of rotation of the model. Assuming that the angle between the line connecting the center of gravity of the middle section of the model G with the model's axis of rotation (actually a point in two dimensions) and the x-axis direction is β, and the distance from the center of gravity of the middle section of the model to the axis of rotation is r, the inertial force of the middle section of the airfoil model can be obtained,

$$|F_i| = mr\dot{\alpha}^2 \tag{3}$$

Then the aerodynamic force of the middle section is $F = F_b - F_i$, where F_b is the measured value of the aerodynamic balance. Under the condition of two-dimensional motion, the components of the aerodynamic forces in the x- and y-axis directions, i.e., the normal force Y and the tangential force X, are represented as

$$Y = Y_b - Y_i = Y_b + |F_i| \sin \beta \tag{4}$$

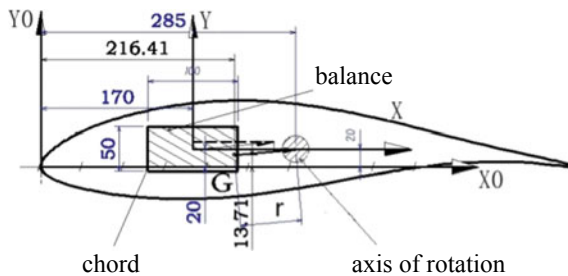$$X = X_b - X_i = X_b + |F|_i \cos \beta \tag{5}$$

Fig. 5 Sectional structure diagram of the middle section of the model (the center of gravity G of the model not on the axis of rotation of model)

Finally, the calculated normal force Y and tangential force X are converted to the model wind axis system, and the final results of the dynamic lift L and drag D can be obtained as

$$L = Y \cos\alpha - X \sin\alpha$$
$$D = Y \sin\alpha + X \cos\alpha$$

(6)

where $L, D, \alpha, \dot{\alpha}$ are the model's lift, drag, and transient angle of attack of pitching motion and its first derivative with respect to time t respectively, and the subscripts b and i represent the balance measuring results and the amount of inertia.

The lift, drag and pitching moment calculated by formulae (2) and (6) are translated to the 1/4 chord point of the airfoil model, and nondimensionalized by the flow dynamic pressure q, the reference area s of the middle section of the model and the chord length c of model to obtain the lift, drag and pitching moment coefficients.

4 Data Processing and Analyses

4.1 Data Filtering and Averaging Processing

The cutoff frequency of the physical low-pass filter used in this study is 5 kHz. Generally, in large-amplitude ($\alpha \geq 10°$) oscillation motion experiments, the 5 or 6 times harmonic components of the oscillation frequency must be taken into account. The amplitudes of pitching oscillation of airfoil studied in this paper are all greater than $10°$, and the maximum frequency of pitch oscillation that can be achieved in the experiments is 2.188 Hz. Therefore, the cut-off frequency of data digital low-pass filtering should be set to greater than 13 Hz.

The analysis of the measuring data shows that the force measuring signal contains a larger signal value with a frequency in the range of 16–60 Hz. By analyzing and comparing the data with different cutoff frequencies, it is determined that a digital low-pass filter with cutoff frequencies of 16 Hz for normal and tangential forces and 8 Hz for pitching moment is used for the force measurement. A Chebyshev filter with zero phase displacement is designed to ensure the phase consistency of the forces and pitching moments before and after filtering. Unless otherwise specified, the result data is the result of filtering with this Chebyshev filter. The data of multiple periods are averaged as the final result of a complete period.

4.2 Calculation of the First and Second Derivatives of the Angle of Attack with Respect to Time

A high-precision angle sensor is installed on the model, and the dynamic data acquisition system is used to collect the transient changes of the angle of attack over time in the experiment. In order to eliminate the error caused by the gap of the model motion driving mechanism, a designed model motion law formula is adopted as follows

$$\alpha = \alpha_0 + A \sin(2\pi f t + \varphi) \tag{7}$$

to fit the collected angle of attack to get the actual value of α_0, A, f, φ, and substitute these value into formula (7) as the actual model motion law formula. And adopt

$$\dot{\alpha} = 2\pi f A \cos(2\pi f t + \varphi)$$
$$\ddot{\alpha} = -(2\pi f)^2 A \sin(2\pi f t + \varphi) \tag{8}$$

to calculate the first and second derivatives of angle of attack α with respect to time, $\dot{\alpha}$ and $\ddot{\alpha}$, where α_0, A, f, φ are the average angle of attack, the amplitude of the angle of attack, the frequency, and the initial phase of the airfoil pitching oscillating motion respectively.

5 Result Analyses

5.1 The Impact of Reduced Frequency

Figure 6 shows the dynamic aerodynamic characteristics of the oscillating airfoil at different reduced frequencies for average angle of attack $\alpha_0 = 15°$, amplitude $A = 15°$ and wind speed $V = 25$ m/s with natural transition of airfoil surface flow. The frequencies in the figure is $f = 0.531, 0.995, 1.326, 1.989$ respectively, which correspond to the reduced frequency $k = 0.04, 0.075, 0.1, 0.15$, respectively. It can be clearly seen from Fig. 6a that as the reduced frequency increases, the airfoil stall is delayed, the reattachment process is also delayed when descending, and the area of the hysteresis loop increases, which is in line with the general law of the dynamic experimental results. It can be seen from Fig. 6b, c that the drag coefficient increases, the pitch moment coefficient near the maximum angle of attack decreases with the increase of the reduced frequency, and the absolute value of its negative value is larger. In the range indicated by the dash line in the figure, the pitching moment coefficient decreases with the increase of the reduced frequency when going up, and increases with the increase of the reduced frequency when going down.
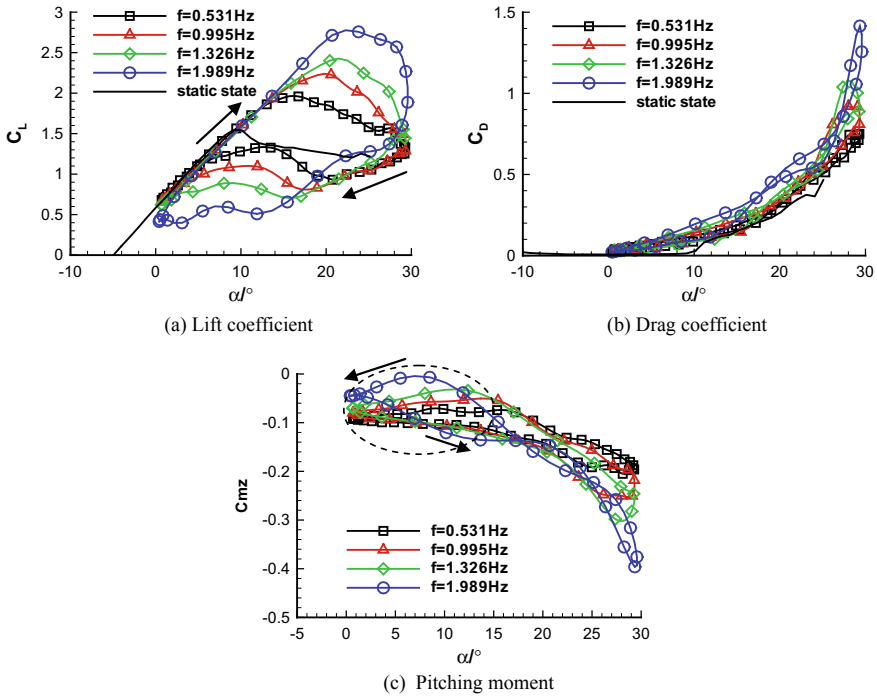
(a) Lift coefficient

(b) Drag coefficient

(c) Pitching moment

Fig. 6 Dynamic aerodynamic characteristics at different frequencies ($\alpha_0 = 15°$, $A = 15°$, $V = 25$ m/s)

5.2 Influence of Amplitude

Figure 7 gives the experimental results of the pitching oscillation of airfoil model with the parameters of average angle of attack $\alpha_0 = 15°$, wind speed $V = 25$ m/s, frequency $f = 0.531$, reduced frequency $k = 0.04$ which the amplitudes are $A = 10, 12, 15°$ respectively. It is shown in Fig. 7 that as the amplitude of the oscillating motion increases, the hysteresis loops of the lift coefficient and the pitch moment coefficient increase.
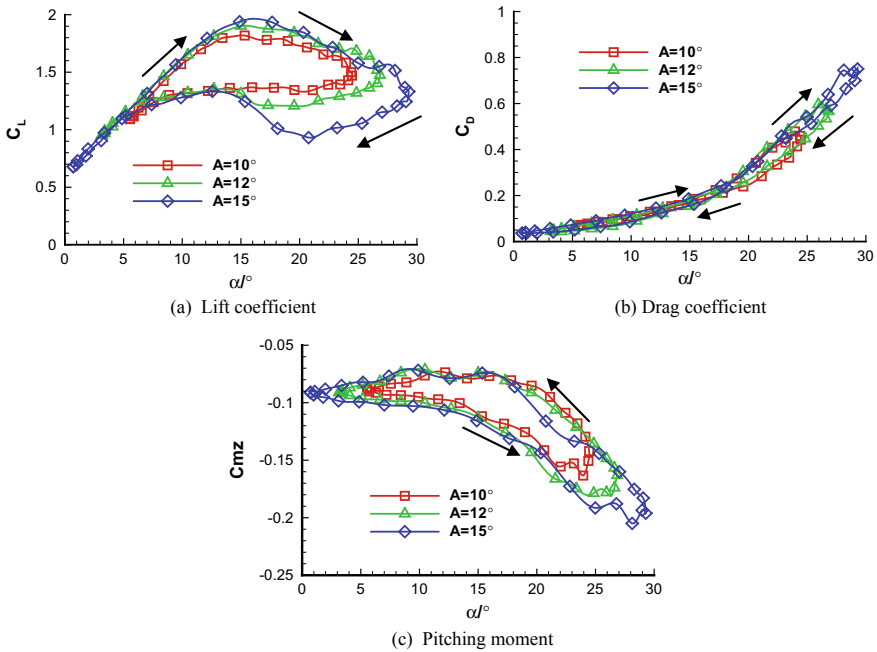
(a) Lift coefficient

(b) Drag coefficient

(c) Pitching moment

Fig. 7 Dynamic aerodynamic characteristics of different amplitudes ($\alpha_0 = 15°$, $V = 25$ m/s, $k = 0.04$)

5.3 Influence of Reynolds Number

In order to investigate the influence of Reynolds number on the dynamic aerodynamic performance of airfoil, Fig. 8 gives the experimental results of the pitching oscillation of airfoil model with the parameters of average angle of attack $\alpha_0 = 15°$, wind speed $V = 25$ m/s, reduced frequency $k = 0.075$, which the Reynolds number are $Re = 1.0, 1.6, 1.8, 2.0, 2.2 \times 10^6$ respectively. In Fig. 8a, it can be clearly seen from the area indicated by the elliptical dashed line that in the downward process, the lift recovery advances, and the hysteresis loop decreases with the increase of the Reynolds number. Reynolds number has no obvious influence on drag coefficient and pitch moment coefficient hysteresis loops. These conclusions are the same as these obtained by Xia YS (10) in the dynamic pressure test of NACA0012 airfoil in 1991 on the whole, but there are the differences somewhat on the shape of lift hysteresis loops.
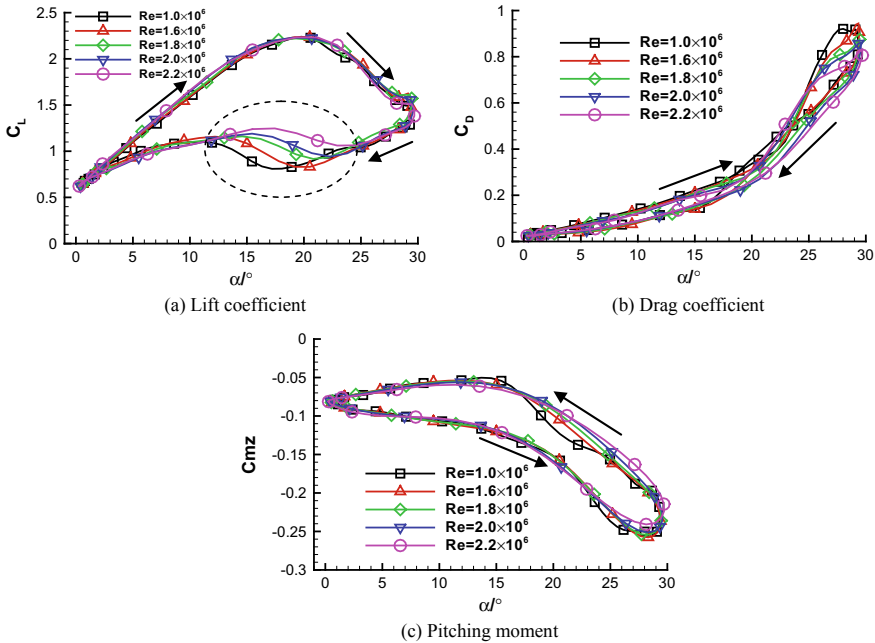
(a) Lift coefficient

(b) Drag coefficient

(c) Pitching moment

Fig. 8 Dynamic aerodynamic characteristics of different Reynolds numbers ($\alpha_0 = 15°$, $A = 15°$, $k = 0.075$)

5.4 Effect of Average Angle of Attack

Figure 9 gives the experimental results of the pitching oscillation of airfoil model with the parameters of amplitude $A = 15°$, wind speed $V = 25$ m/s, frequency $f = 0.531$ and reduced frequency $k = 0.04$, which the average angles of attack are $\alpha_0 = 0°, 5°, 10°, 15°$ respectively. It can be clearly seen from Fig. 9 that when the average angle of attack $\alpha_0 = 0°, 5°, 10°$ gradually increases, the stall angle of attack gradually increases, and the maximum lift coefficient also increases. But, when the average angle of attack further increases to $\alpha_0 = 15°$, the stall angle of attack remains unchanged and is $16°$, the maximum lift coefficient is also unchanged. As the average angle of attack increases, the lift hysteresis loop increases. When the angle of attack approaches the lower limit, the hysteresis loop also appears, and the drag coefficient has a more obvious hysteresis loop near the lower limit of the angle of attack. When the average angle of attack increases successively, $\alpha0 = 0°, 5°, 10°, 15°$, the pitch moment coefficient hysteresis loop moves in the direction of increasing angle of attack, and the value of the minimum pitch moment coefficient decreases. At the average angle of attack of $\alpha_0 = 0°$, since the minimum angle of attack is already smaller than the negative static stall angle of attack, it enters a negative stall, forming the "8"-shaped hysteresis loop of lift and pitching moment coefficients. Since the average angle of attack controls the range of angle of attack
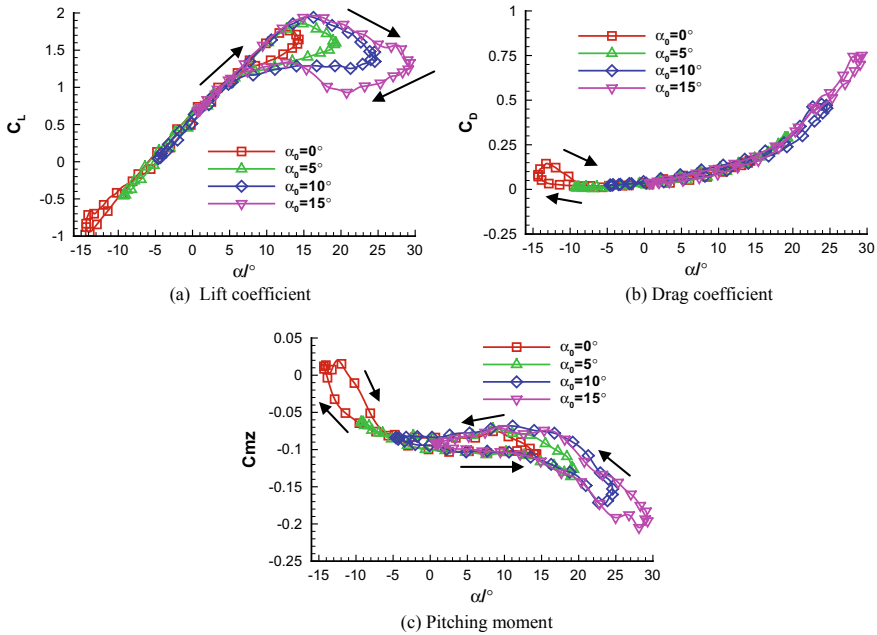
(a) Lift coefficient

(b) Drag coefficient

(c) Pitching moment

Fig. 9 Dynamic aerodynamic characteristics of the different average angle of attack ($A = 15°, f = 0.531, V = 25$ m/s)

of the oscillating airfoil, when the average angle of attack increases, the oscillation range more enters the positive deep stall zone, and the hysteresis loops of lift and pitching moment coefficient moves and increases in the direction of the increasing angle of attack. Therefore, the angle of attack exceeding the positive or negative stall angle of attack is a necessary condition for a large hysteresis loop to form.

6 Conclusions

The main research conclusions are:

1. The angle of attack exceeding the positive or negative stall angle of attack is a necessary condition for the lift coefficient and pitching moment coefficient to produce a large hysteresis loops.
2. As the oscillation reduced frequency increases, the dynamic stall is delayed, the lift coefficient hysteresis loop increases, the drag coefficient increases, and the pitch moment coefficient near the maximum angle of attack decreases, and the absolute value of its negative value is greater. When the angle of attack is less than the static stall angle of attack or exceeds a small range of angle of attack, with the increase of the reduced frequency, the pitching moment coefficient

decreases when the oscillating motion moves upward, and increases when it moves downward.

3. As the oscillation amplitude increases, the hysteresis loops of the lift coefficient and pitch moment coefficient increase.

4. As the average angle of attack increases, the airfoil angle of attack enters the positive stall zone more, the lift coefficient hysteresis loop increases, and the minimum pitch moment coefficient decreases.

5. The Reynolds number has no obvious effect on the drag coefficient and pitch moment coefficient hysteresis loop, and has a small effect on the lift coefficient. In the downward process, as the Reynolds number increases, the lift recovery advance and then the hysteresis loop decreases.

References

1. Carr LW (1988) Progress in the analysis prediction of dynamic stall. J Aircr 25(1):6–17
2. Leishman JG (2000) Principles of helicopter aerodynamics. Cambridge University Press, Cambridge, pp 302–318
3. Conlisk AT (2001) Modern helicopter rotor aerodynamics. Prog Aerosp Sci 37(5):419–476
4. Ham ND (1968) Aerodynamic loading in a two-dimensional airfoil during dynamic stall. AIAA J 6(10):1927–1934
5. McCroskey WJ, Pucci SL (1982) Viscous-inviscid interaction on oscillating airfoil in subsonic flow. AIAA J 20(2):167–174
6. Carr LW, McAlister KW, McCroskey WJ (1977) Analysis of the development of dynamic stall based on oscillating airfoil experiments. National Aeronautics and Space Administration, Washington D. C. NASA TN D-8382
7. McAlister KW, Carr LW, McCroskey WJ (1978) Dynamic stall Experiments on the NACA0012 Airfoil. National Aeronautics and Space Administration, Washington D. C. NACA TP 1100
8. Conger RN, Ramaprian BR (1994) Pressure measurements on a pitching airfoil in a water channel. AAIA J 32(1):108–115
9. Piziali RA (1994) 2-D and 3-D oscillating wing aerodynamics for a range of angles of attack including stall. National Aeronautics and Space Administration, Washington D. C. NASA TM 4632
10. Xia YS et al (1996) Dynamic of stall characters of NACA0012 airfoil and investigations of dynamic pressure measure methods. Acta Aeronautica et Astronautica Sinica. 17(7):25–30
11. Hui ZH, Wang L, Xu Q (2012) Dynamic pressure measurement techniques on wind turbine air-foil. J Experiments Fluid Mech 26(4):6–10
12. Panda J, Zaman KBMQ (1994) Experimental investigation of the flow field of an oscillating airfoil and estimation of lift from wake surveys. J Fluid Mech 265:65–95
13. Werner P et al (1996) Experimental and numerical investigations of dynamic stall on a pitching airfoil. AIAA J 34(5):982–989
14. Oshima H, Ramapian BR (1997) Velocity measurements over a pitching airfoil. AIAA J 35(1):119–126
15. Wang Q, Zhao QJ, Zhao GQ (2014) PIV experiments on flow field characteristic of rotor airfoil dynamic stall and modifications of L-B model. Chinese J Theoret Appl Mech 46(4):631–635
16. Tang RY, Hua XM, Wu SJ (1992) Experimental study of dynamic stall on an oscillating airfoil. J Nanjing Aeronaut Inst 24(5):506–512
17. Tsang KYK (2006) Direct force measurements of a two-dimensional airfoil undergoing dynamic stall. Hong Kong Polytechnic University, Hong Kong, pp 1–125

18. Rival D, Tropea C (2010) Characteristics of pitching and plunging airfoils under dynamic-stall conditions. J Aircraft 47(1)
19. Lin YF et al (2012) Experimental investigation of rotor airfoil dynamic stall characteristics. Aeronaut Sci Technol Special Helicopter Technol 2012(4):25–28
20. Jiao YQ et al (2020) Three-section airfoil experimental model with integral frame for dynamic force measurement in wind tunnel. China National Intellectual Property Administration, Peking. 2020–6–9. CN201921940956.4[P]